



# Heterogeneous electro-Fenton system using Fe-MOF as catalyst and electrocatalyst for degradation of pharmaceuticals

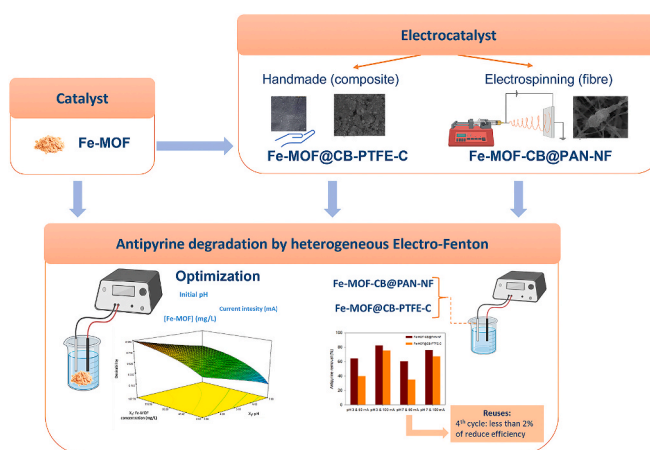
Antía Fdez-Sanromán<sup>\*</sup>, Marta Pazos, M. Angeles Sanromán, Emilio Rosales

CINTECX, Universidade de Vigo, Grupo de Bioingeniería y Procesos Sostenibles, Departamento de Ingeniería Química, Campus Lagoas-Marcosende, 36310, Vigo, Spain

## HIGHLIGHTS

- Fe-MOF as heterogeneous catalyst for electro-Fenton process.
- Optimization of key parameters for antipyrine degradation by Fe-MOF electro-Fenton.
- Fe-MOF utility for the synthesis of electrocatalyst: Composite and electrospinning fibre.
- Composite green synthesis showed great strength and high removal efficiency.
- Fiber Fe-MOF exhibited good performance, high stability and durability.

## GRAPHICAL ABSTRACT



## ARTICLE INFO

Handling Editor: Sergi Garcia-Segura

### Keywords:

Antipyrine  
Electrode synthesis  
Fe-MOF  
Heterogeneous electro-fenton  
Response surface methodology

## ABSTRACT

In recent years, heterogeneous electro-Fenton processes have gained considerable attention as an alternative to homogeneous processes. In this context, the aim of this study is the use of a commercial iron metal-organic framework (Fe-MOF), Basolite® F-300, as a base material for the design of a heterogeneous electro-Fenton treatment system for the removal of antipyrine. Initially, the catalyst was applied as powder in aqueous solution and three key parameters of the electro-Fenton process (pH, Fe-MOF concentration and current density) were evaluated and optimized by a Central Composite Design Face Centred (CCD-FC) using antipyrine removal and energy consumption as response functions. Near complete antipyrine removal (94%) was achieved under optimal conditions: pH 3, Fe-MOF 157.78 mg/L and current density 6.67 mA/cm<sup>2</sup>, obtaining an energy consumption of 0.29 W·h per mg of antipyrine removed. Later, two electrocatalysts (Fe-MOF functionalized cathodes), prepared by different Fe-MOF immobilisation approaches (composite of carbon black/polytetrafluoroethylene or by electrospinning on Ni foam), were synthesized. Their characterisation showed notable Fe-MOF incorporation into the material and favourable properties as electrocatalysts. Both Fe-MOF functionalized cathodes were evaluated in the removal of antipyrine at different pH (acidic and natural) and

<sup>\*</sup> Corresponding author.

E-mail addresses: [antia.fernandez.sanroman@uvigo.es](mailto:antia.fernandez.sanroman@uvigo.es) (A. Fdez-Sanromán), [mcurras@uvigo.es](mailto:mcurras@uvigo.es) (M. Pazos), [sanroman@uvigo.es](mailto:sanroman@uvigo.es) (M.A. Sanromán), [emilirov@uvigo.es](mailto:emilirov@uvigo.es) (E. Rosales).

<https://doi.org/10.1016/j.chemosphere.2023.139942>

Received 1 June 2023; Received in revised form 7 August 2023; Accepted 22 August 2023

Available online 25 August 2023

0045-6535/© 2023 The Authors. Published by Elsevier Ltd. This is an open access article under the CC BY-NC license (<http://creativecommons.org/licenses/by-nc/4.0/>).

current density (27.78 and 55.56 mA/cm<sup>2</sup>), achieving in the best conditions removal levels around 80% in 1 h without any operational problems. In addition, several intermediates generated during the treatment were identified and their toxicity estimated. According to the obtained results, the degradation compounds have less toxicity than the parent compounds, confirming the effectiveness of the treatment.

## 1. Introduction

A societal demand that has become increasingly important over the last few years is ensuring the availability and sustainable management of water that is threatened by persistent pollutants. The treatment of wastewater can be tackled by different physical and/or chemical alternatives, but electrochemical advanced oxidation processes (electro-Fenton, photoelectro-Fenton) have arisen as feasible options.

It is well-known that electro-Fenton is an efficient technology for the degradation of organic contaminants in wastewater that are recalcitrant. Several studies conducted up to date suggested that this technique can be ameliorated by the use of heterogeneous catalysts, which may improve Fenton's reactions because of: i) their higher activity at a wide range of pH conditions; ii) higher stability; and iii) capability of being reused than commonly used soluble iron salts (Casado, 2019; Poza-Nogueiras et al., 2018). Fenton reactions are promoted at catalyst surfaces by the generation of oxidant radicals, mainly hydroxyl radicals. These radicals generated by Fenton-related processes can degrade a wide range of pollutants such as pesticides (Fdez-Sanromán et al., 2020), polycyclic aromatic hydrocarbons (Gou et al., 2022), pharmaceutical (Cuervo Lumbaque et al., 2021) and personal care products (Pisharody et al., 2022).

In heterogeneous electro-Fenton processes, insoluble iron-containing species are dispersed randomly in the aqueous medium or supported on a variety of materials or functionalized cathodes (electrocatalysts) for *in-situ* generation of Fenton's reagents. In both cases, catalysts are easily handled, stored safely, and recovered from sewage effluents (Fdez-Sanromán et al., 2021; Lama et al., 2022; Poza-Nogueiras et al., 2018, 2022). In recent years, the development of these heterogeneous electro-Fenton treatments has attracted great interest in the treatment of synthetic and real wastewater (Brillas, 2022), and suggests that the new cornerstone will be the search for new materials and composites that improve current processes for application in real contaminated environments. Among them, metal-organic frameworks (MOF), especially iron-MOF (Fe-MOF) and Fe-MOF derived carbons, characterized by highly tuneable porosity, large surface area, and open metal sites, have attracted the attention of the scientific community as adsorbents or a catalysts (Du and Zhou, 2021; Fdez-Sanromán et al., 2022; Sirés and Brillas, 2021). Iron-carbon composites derived from MOFs provided excellent performance in both suspension catalysts and modified cathodes for environmental remediation (Du et al., 2022, 2023), but more studies are needed to advance in the improvement of these materials for electro-Fenton processes.

Herein, this study is focused on the development of a Fe-MOF based heterogeneous electro-Fenton treatment of pharmaceutical compounds using antipyrine as target pollutant. This pharmaceutical product is an anti-inflammatory analgesic drug commonly used for treating fever, headaches, and general pain (Ouiriemmi et al., 2022). As result of its limited adsorption in the human body, antipyrine is released in significant amounts and, thus, commonly found into aquatic environments (Gomes et al., 2019; Reddersen et al., 2002). It was estimated that conventional wastewater treatment plants remove only about 30% of antipyrine from their effluent (Deblonde et al., 2011). Because of the potential harm it can cause in aquatic systems, it is important to search technologies that can remove this pollutant at low concentrations.

For this purpose, the evaluation of a commercial Fe-MOF, called Basolite® F-300, as heterogeneous catalysts in aqueous media or electrocatalysts using Fe-MOF functionalized cathodes was performed. Initially, the heterogeneous electro-Fenton process by adding Fe-MOF to

the reaction medium was studied and optimized by using a Central Composite Design Face Centred (CCD-FC). Three key parameters (pH, Fe-MOF concentration and current density), using antipyrine removal and energy consumption as response functions, were evaluated. In addition, this Fe-MOF was used to fabricate two electrocatalysts (Fe-MOF functionalized cathodes): i) composite by mixing with carbon black (CB) and polytetrafluoroethylene (PTFE); or ii) by direct application of electrospinning technology. Both Fe-MOF functionalized cathodes were characterized and investigated for their ability to degrade antipyrine, to determine their behaviour, and their key advantages.

## 2. Materials and methods

### 2.1. Reagents

All reagents used in the synthesis and degradation process can be found in the [Supplementary material](#).

### 2.2. Electrocatalyst preparation

Two types of Fe-MOF functionalized cathodes were produced by applying two different immobilisation techniques: i) Fe-MOF was incorporated into a composite containing CB and PTFE, resulting an electrocatalyst named Fe-MOF@CB-PTFE-C, and ii) electrospinning by embedding Fe-MOF into the internal filaments of the polyacrylonitrile (PAN) fibre, which was supported on Nickel Foam (NF), referred to as Fe-MOF-CB@PAN-NF.

#### 2.2.1. Fe-MOF@CB-PTFE-C

A doughy solid was prepared by the mixture of CB and PTFE solution as an organic binder with a mass percentage of 40 wt% adapted from Cruz del Álamo et al. (2023). For this reason, the quantities used to make this mass were: 0.16 g CB, 0.05 g PTFE and 0.5 g ultrapure water. Afterwards, 0.2 g Fe-MOF was added to generate the composite, which was hand-pressed using a mould to produce a rectangular flat-plate electrode with a surface area of 2 cm<sup>2</sup> and a thickness of 2 mm. Finally, Fe-MOF@CB-PTFE-C electrode was dried at 80 °C for 2 h. Another control composite electrode (CB-PTFE-C) was also synthesized using the same procedure without Fe-MOF.

#### 2.2.2. Fe-MOF-CB@PAN-NF

In the electrospinning synthesis, it is essential to establish the appropriate ratio of reagents. Therefore, preliminary experiments were conducted using varying concentrations: PAN (5–7%), CB (4–6%), and Fe-MOF (2–3%). Firstly, PAN was dissolved in DMF at 60 °C, and then thoroughly mixed with Fe-MOF for 12 h using magnetic stirring at 400 rpm. Subsequently, CB was added, and the mixture was further stirred for 24 h at 400 rpm. The resulting solution was sonicated using a Fisherbrand FB11203 sonicator (Fisher Scientific, Spain) for 30 min and fed through a stainless needle using a syringe pump at a rate ranging from 0.3 to 1.4 mL/h. To fabricate Fe-MOF-CB@PAN-NF nanofiber mats, an aluminium foil collector with NF was positioned at a distance of 10–20 cm from the needle, and voltages between 13 and 20 kV were applied. This process produced various Fe-MOF-nonwoven mats of PAN nanofibers on the NF. Additionally, to highlight the differences, PAN fibres were also synthesized without the incorporation of Fe-MOF, using PAN concentrations within the range of 5–7%. The concentration range of the reagents was chosen because it was impossible to synthesize fibres with other combinations of these compounds. A reason for this could be due

to the density and rheology of the solution, which makes it impossible to move the solution or make an electrospray process.

## 2.3. Characterisation

### 2.3.1. Physicochemical characterisation

X-ray diffraction (XRD) was performed on a Siemens D5000 diffractometer (Ks Analytical Systems, United States) to study the crystalline composition of the Fe-MOF functionalized cathode. Scanning Electron Microscopy and Energy Dispersive Spectrometry (SEM-EDS) were conducted on a JEOL JSM6010LA (Jeol, Japan) equipped with an EDS Oxford AZtecOne SEM (Oxford Instruments, England). To identify all functional groups and bindings formed inside the electrodes, Fourier transform infrared spectroscopy (FTIR) was carried out on a Nicolet 6700 spectrometer (Thermo Fisher Scientific Inc., United States). A thermobalance (SETSYS Evolution 1750, Setaram, France) was used to perform the thermogravimetric analysis (TGA) of the electrodes and fibres. About 11 mg of sample were heated up to 800 °C (10 °C/min) under constant air flow (30 mL/min). All equipment mentioned above was used on *Centro de Apoyo Científico-Tecnológico a Investigación* (CACTI, University of Vigo, Spain). The hydrophobicity/hydrophilicity of the two electrocatalysts was assessed by water contact angle. A goniometer Mobile Drop Analyzer (Krüss GmbH, Germany) was used to measure the contact angle of one drop of ultrapure water on the surface of electrocatalysts. DSA2 software (Krüss GmbH, Germany) was utilized to analyse the drop shape. Water contact angle measurements were performed after water drop deposition with intervals of 30 s for 5 min.

### 2.3.2. Electrochemical characterisation

Cyclic voltammetry (CV) was used to determine the electrochemical properties of the functional catalysts. For this purpose, a potentiostat PGSTAT302 N (Metrohm Autolab, The Netherlands) working with a three-electrode cell was used with an Ag/AgCl reference electrode, a platinum wire (0.5 × 100 mm) as the counter electrode, and the functional electrode as working electrode. CV was performed under a potential between −1.0 and 1.0 V, and it has been carried out in a 100 mL sodium sulphate (Na<sub>2</sub>SO<sub>4</sub>) solution (0.5 M).

## 2.4. Degradation assays

### 2.4.1. Antipyrine degradation using Fe-MOF as catalyst

In this study, the electro-Fenton process was carried out in a glass cylindrical reactor (150 mL) with magnetic stirring (300 rpm) containing 50 mL of antipyrine (50 mg/L), which contained Na<sub>2</sub>SO<sub>4</sub> (10 mM) as electrolyte. Before starting the experiment, solution pH was adjusted with 0.1 M H<sub>2</sub>SO<sub>4</sub> to the desired value, if required, and the solution was saturated with air by constant bubbling (0.75 L/min). Boron Doped Diamond (BDD) was selected as anode and NF or Carbon Felt (CF) were evaluated as cathodes, all with the same dimensions (5 × 2.5 × 0.2 cm). Initially, the system was operated at current density 13.33 mA/cm<sup>2</sup>, pH 7 and Fe-MOF 76 mg/L, which will be modified in the optimization.

The treatment efficiency was assessed considering antipyrine removal and energy consumption (Equations (1) and (2)).

$$\text{Antipyrine removal (\%)} = 100 \cdot ((C_0 - C_t) / C_0) \quad (1)$$

$$\text{Energy consumption (W} \cdot \text{h)} = I \cdot V_m \cdot t \quad (2)$$

where  $C_t$  corresponds to the concentration of antipyrine during the experiment (mg/L),  $C_0$  to its initial concentration (mg/L),  $I$  to the current intensity (A),  $V_m$  is the average voltage of the experiment and  $t$  sample time which was always 1 h.

### 2.4.2. Antipyrine degradation using Fe-MOF functionalized cathodes

A similar experimental setup that described above was used in this system with a BDD anode and different Fe-MOF functionalized cathodes (Fe-MOF@CB-PTFE-C or Fe-MOF-CB@PAN-NF) (1.7 × 1.2 × 0.2 cm)

positioned at 2 cm and a certain current density (55.56 mA/cm<sup>2</sup> or 27.28 mA/cm<sup>2</sup>) was applied.

## 2.5. Analytical determination

### 2.5.1. Pollutant concentration

HPLC Agilent 1260 (equipped with a Diode Array Detector at 242 nm) was used to measure antipyrine degradation in both electro-Fenton experiments. Chromatographic separation was carried out using a Zorbax Eclipse, XDB-C8, column (dimensions: 150 × 4.6 mm, 5 μm, Agilent Technologies, USA) at room temperature. The mobile phase, 1.5% acetic acid and acetonitrile (90:10 v/v) was pumped at a flow rate of 1 mL/min. Each sample was filtered through 0.45 mm PVDF filters before chromatographic analysis.

### 2.5.2. Hydrogen peroxide concentration

Hydrogen peroxide was detected by spectrophotometry following the formation of titanium (IV)-peroxide complexes at 400 nm, in the electro-Fenton experiments. Accordingly, 2 mL of solution was combined with 0.25 mL H<sub>2</sub>SO<sub>4</sub> (1:17), 0.20 mL of 50 g/L potassium titanium oxide oxalate dihydrate and 0.05 mL of water. After 5 min, the mixture's absorbance was measured.

### 2.5.3. Identification of degradation products

To determine the degradation pathway of the target pollutant, Liquid Chromatography-Mass Spectrometry (LC-MS) technique was used through a Hewlett-Packard 1050 with a MS Detector Hewlett-Packard 5989 B (C.A.C.T.I., University of Vigo, Spain). In this case, the used column was the Zorbax Eclipse Rapid Resolution XDB-C18 (dimensions: 2.1 × 100 mm, 1.8 μm, Agilent Technologies, USA).

## 2.6. Statistical analysis and optimization

The electro-Fenton process using the Fe-MOF as a catalyst was optimized by a response surface methodology (RSM) with CCD-FC. The system consisted of a 2<sup>3</sup> with three factors evaluated at two levels: initial pH,  $X_1$ , 3 and 7; Fe-MOF concentration,  $X_2$ , 2.63 and 157.78 mg/L; and current density,  $X_3$ , 6.67 and 13.33 mA/cm<sup>2</sup>. Two responses were selected: percentage of antipyrine removal and energy consumption (for more information see supplementary section). The model's statistical analysis and analysis of variance (ANOVA) were conducted using Design Expert® 8.0.0 software (Stat-Ease Inc. Minneapolis, USA).

## 2.7. Toxicity

Toxicity Estimation Software Tool (TEST) version 5.1.2 (US Environmental Protection Agency) was used to estimate antipyrine by-product toxicity. These predictions were realized from chemical structures' physical properties through quantitative structure-activity relationships (QSAR) (Sai et al., 2023). The toxicity endpoints were assessed at: (i) the 50% lethal concentration (LC50) of Fathead minnows (*Pimephales promelas*) in 4 days (96 h), (ii) the LC50 of *Daphnia magna*, a water flea, in 48 h, (iii) the amount of the chemical that, when orally ingested, is lethal to half (LD50) of the rats, called oral rat LD50. A consensus-based QSAR approach was used to study the impact of input chemicals on model parameters.

## 3. Results and discussion

### 3.1. Degradation of antipyrine by Fe-MOF electro-Fenton process

#### 3.1.1. Selection of electrodes

Initially, the selection of the cathode material was carried out in the Fe-MOF electro-Fenton process considering NF-BDD and CF-BDD (Fig. S1) as alternatives cathode-anode (subsection 2.4.1). Before the electro-Fenton degradation experiments, adsorption experiments on Fe-

MOF were required as control in order to determine the possible removal of antipyrine by adsorption. However, no antipyrine adsorption on the Fe-MOF was detected and, thus, the removal detected in the electro-Fenton in presence of Fe-MOF is due to the AOP process performed. Both electrodes' combinations exhibited a different degradation rate, with NF-BDD achieving a higher level of removal (around 55%) than CF-BDD (47%). The kinetic of the reaction was also studied by adjusting it to a first or second order model. First model fitted well to the data ( $R^2 > 0.99$ ) showing a higher kinetic constant for NF-BDD system ( $0.014 \text{ min}^{-1}$ ) in comparison with CF-BDD ( $0.0115 \text{ min}^{-1}$ ). The difference could be explained due to the hydrogen peroxide production levels in the cathode and consequent hydroxyl radicals' production by Fenton's reaction. This fact was confirmed by measuring the hydrogen peroxide production where it was confirmed that by using NF-BDD a higher hydrogen peroxide production of  $11.04 \text{ mg/L}$  (Fig. S2) was achieved (Sun et al., 2018). Therefore, the NF-BDD configuration was selected as the best alternative with a higher removal and degradation rate compared to anodic oxidation (Fig. S3).

### 3.1.2. Experimental design model

Once the electrochemical configurations were selected, the treatment was improved by studying the influence of key parameters in the degradation process using an RSM: initial pH ( $X_1$ ), Fe-MOF concentration ( $X_2$ ) and current density ( $X_3$ ). A two-level-three-factor CCD-FC approach was applied resulting in 19 runs with antipyrine's removal and energy consumption as responses (Table S1).

ANOVA analysis was performed for each response (Tables S2 and S3). First, the antipyrine's removal response was analysed. It was demonstrated that quadratic model (equation (3)), in which the response is described as a function of the variables as coded factors, fitted well to the experimental results. Thus, the high value of  $R^2$  (0.9927) indicates a high correlation between the predicted and experimental values. In addition, the predicted  $R^2$  (0.8954) was in reasonable agreement with the adjusted  $R^2$  (0.9855).

$$\text{Antipyrine removal (\%)} = 73.44 - 7.70 \cdot X_1 + 8.38 \cdot X_2 + 2.25 \cdot X_3 - 0.92 \cdot X_1 \cdot X_2 - 1.08 \cdot X_1 \cdot X_3 - 0.22 \cdot X_2 \cdot X_3 + 0.70 \cdot X_1^2 - 2.02 \cdot X_2^2 + 1.02 \cdot X_3^2 \quad (3)$$

The significant terms were  $X_1$ ,  $X_2$ ,  $X_3$ ,  $X_1 \cdot X_2$ ,  $X_1 \cdot X_3$  and  $X_2^2$ . Thus, the increase in catalyst concentration and current density favoured pollutant removal while the increase in pH had the opposite behaviour (Figs. S4a and S4b).

With respect to the other studied response, energy consumption, there was also a good correlation (Table S2) with a quadratic model  $R^2$  (0.9924) and, a good agreement between the predicted  $R^2$  (0.9847) and the adjusted correlation coefficient  $R^2$  (0.9033). In this case, the coded relation between response and the factors evaluated can be described by equation (4).

$$\text{Energy Consumption (W} \cdot \text{h)} = 1.02 + 0.083 \cdot X_1 - 0.002 \cdot X_2 + 0.47 \cdot X_3 - 0.009 \cdot X_1 \cdot X_2 + 0.015 \cdot X_1 \cdot X_3 + 0.042 \cdot X_2 \cdot X_3 - 0.029 \cdot X_1^2 + 0.079 \cdot X_2^2 - 0.11 \cdot X_3^2 \quad (4)$$

The significant terms of the energy consumption response were  $X_1$ ,  $X_3$ ,  $X_2 \cdot X_3$ ,  $X_2^2$  and  $X_3^2$  with the current density as logically the most important variable in the final energy consumption of the electro-Fenton process. When evaluating the response surface plots corresponding to  $X_1 \cdot X_2$  (Fig. S5a) and  $X_2 \cdot X_3$  (Fig. S5b) terms, the  $X_3$  term is mainly the one that sets the upper (red colour) and lower (blue colour) values of the energy consumption response.

### 3.1.3. Optimization of the degradation process

Once the quadratic model was obtained for each response, it was desired to establish which were the optimal conditions in this NF-BDD electro-Fenton system using Fe-MOF as a catalyst in suspension. To optimize multiple responses and provide the best value of compromise in the desirable joint response (Fig. S6), the desirability function was

used. It was established as conditions the maximum pollutant removal and minimum energy consumption. The optimum conditions resulted in pH 3, the current density of  $6.67 \text{ mA/cm}^2$  and Fe-MOF concentration of  $157.78 \text{ mg/L}$ . Operating at these conditions it was possible to eliminate up to 86.97% and a consumption of  $0.196 \text{ W} \cdot \text{h}$  per mg of antipyrine removed was obtained. Under these conditions, the model predicted an antipyrine removal around 87.09% after 1 h with a consumption of  $0.194 \text{ W} \cdot \text{h}$  per mg of antipyrine removed, so the relative error was 0.14% and 0.95%, respectively. These results highlight the efficiency of this proposed process in comparison to others such as the photo-degradation, in which for complete removal was achieved after 6 h (Peñas-Garzón et al., 2020) or ozonation in presence of nanoparticles catalyst ( $\text{Fe}_3\text{O}_4/\text{SiO}_2/\text{CeO}_2$ ) with removal rate of 88% after 2 h (Chen et al., 2021).

Even though the heterogeneous catalyst gave promising results, it presented some operational difficulties due to its small size, which makes it difficult to retain inside the electrochemical cell in flow systems. With the aim to avoid these operational problems, improve its life cycle and sustainability, and facilitate its recovery from aqueous media, Fe-MOF was immobilised by different techniques. The synthesized material was tested as electrocatalyst using a Fe-MOF functionalized cathode without the presence on Fe-MOF into the aqueous media.

## 3.2. Characterisation of Fe-MOF functionalized cathodes

As explained in the previous section, to improve the stability of Fe-MOF, two immobilisation techniques were used to obtain two different types of electrocatalysts used as cathode. Initially, the catalyst was incorporated into a composite electrode containing CB and PTFE resulting in an electrocatalyst Fe-MOF@CB-PTFE-C. While the other immobilisation procedure used electrospinning to adhere the catalyst to the fibre's internal filaments before it was deposited on a NF (Fe-MOF-CB@PAN-NF). After their synthesis, both materials were characterized to determine their suitability for their use as catalyst and cathode.

### 3.2.1. Fe-MOF@CB-PTFE-C

**3.2.1.1. Physicochemical characterisation.** Firstly, the analysis of the Fe-MOF@CB-PTFE-C and the composite without the Fe-MOF (CB-PTFE-C) surface by SEM and the corresponding mapping were carried out (Fig. 1a and b). As can be seen, MOF@CB-PTFE-C showed a relatively smooth surface and presents a homogeneous distribution of carbon, oxygen, and iron confirming the correct fixation of the catalyst in the produced composite in comparison with CB-PTFE-C. Also, the fluorine element was present in the mapping because it is provided by PTFE.

The FTIR spectra of Fe-MOF@CB-PTFE-C is displayed in Fig. 1c. The data confirmed the fixation of the Fe-MOF in the electrocatalyst. It was observed the presence in the composite of conformational environment of Fe-MOF, 1,3,5-benzenetricarboxylate (BTC) linker molecules as vibrations in the  $700\text{--}1720 \text{ cm}^{-1}$  range. Bands placed at  $1191$  and  $1143 \text{ cm}^{-1}$  were assigned to the asymmetric bridge C–O–C and the broad signal observed at  $1023 \text{ cm}^{-1}$  corresponding to O–C stretching of the BTC ligand (Rivera-Torrente et al., 2018). The peaks in the range  $1300\text{--}1700 \text{ cm}^{-1}$  were related to the carboxylate groups indicating BTC coordination to the metal sites (Conde-González et al., 2021).

In addition, the XRD technique allowed for the identification of the presence of Fe-MOF in Fe-MOF@CB-PTFE-C (Fig. 1d). The characteristic peak at  $2\theta = 11^\circ$  from Fe-MOF was not clearly observed, but an increase in this region was shown in comparison with the CB-PTFE-C due to its presence. Due to the Fe-MOF semiamorphous nature, it exhibited non-crystalline solid characteristics (Ursueguía et al., 2020). The peak at  $2\theta = 18^\circ$  was related to the PTFE (Sippel et al., 2013) and  $2\theta = 26^\circ$ , it was a characteristic peak of CB (Lee et al., 2021). Moreover, these two peaks coincided with those reported by Karatas et al. (2022), who prepared a CB electrode using PTFE as a blinder and the reported results for



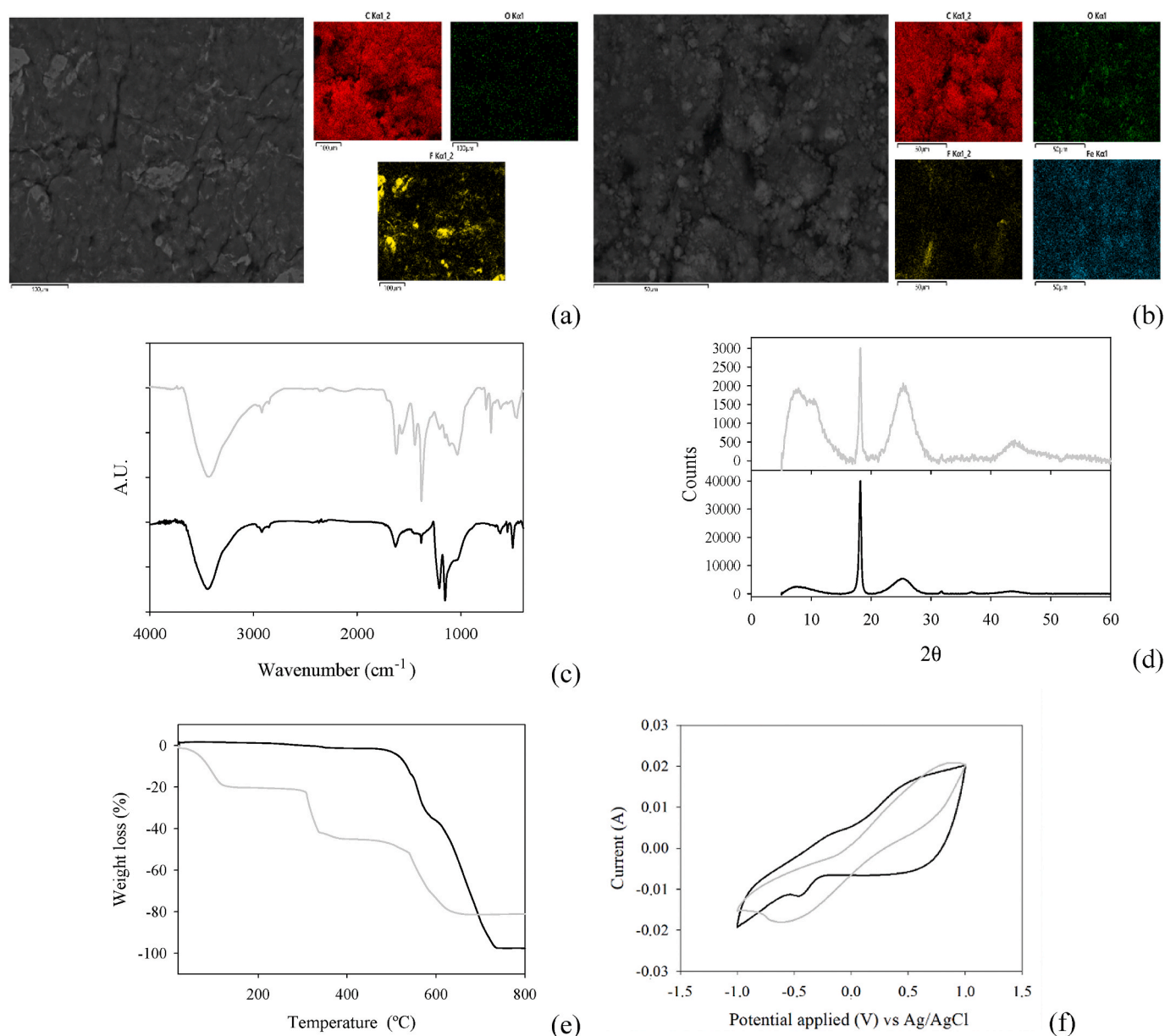


**Fig. 1.** SEM images and corresponding mappings of the composite electrodes (a) CB-PTFE-C and (b) Fe-MOF@CB-PTFE-C; (c) FTIR, (d) XRD, (e) TGA and (f) CV. Black and grey lines represent the results of CB-PTFE-C and Fe-MOF@CB-PTFE-C, respectively.

CB-PTFE-C. As it can be expected these peaks decreased with the presence of the Fe-MOF.

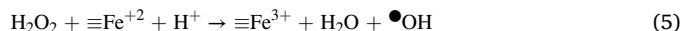
The electrode's stability to possible thermal reactions or physical transformations was analysed by TGA. Fig. 1e shows both composite electrodes undergo multi-stage decomposition. In Fe-MOF@CB-PTFE-C (grey line), its behaviour differed from the composite without catalyst considerably. The first mass loss occurred from 20 °C to 100 °C due to the evaporation of water molecules from the Fe-MOF itself. This drop was not observed on the CB-PTFE-C curve. This mass loss was reported in other works such as Nguyen et al. (2021). In their work they synthesized a novel nanoscale MOF material with Ytterbium and BTC ligands. When performing the TGA analysis they associated the mass loss below 100 °C to the depletion of adsorbed moisture and water molecules bound tightly to organic frameworks. Another mass loss shared with Nguyen et al. (2021) occurred from 300 to 335 °C, and was attributed to organic ligands, including the BTC. The last section of the TGA curve, which was from 500 to 660 °C, was due to the composition of PTFE and CB due to the similarity of the curve in this temperature range. This

association was possible because of works such as Hondred et al. (2013) analysed the degradation kinetics of two widely used fluorocarbon-based polymers, poly (ethylene-*alt*-tetrafluoroethylene) and PTFE. In this study, they analysed the various TGA curves of PTFE obtained at different heating rates. It was found that PTFE shows a one-step degradation process. On CB, the curve obtained from TGA analysis depends mainly on the purity of the carbonaceous material. In normal circumstances, combustion occurs when this analysis was performed with an air atmosphere above 600 °C (Shamsudin et al., 2013). Finally, the differences in mass loss found at temperatures above 700 °C were due to the presence of the iron element, as it was not possible to combust the inorganic part of the Fe-MOF@CB-PTFE-C, as was achieved with CB-PTFE-C.

**3.2.1.2. Electrochemical characterisation.** Once it has been ensured that the catalyst is immobilised on the electrode, it is worthwhile to study the feasibility of its use as an electrocatalyst by studying the effect in the electroactive surface area and its effect on the generation of hydrogen

peroxide by following the cathodic peak attributed to the oxygen reduction. Therefore, a CV study was needed. According to Fig. 1f, when Fe-MOF was absent, a peak higher than  $-0.4$  V appeared, which was associated with hydrogen peroxide production when the potential is applied. This peak has also been identified in several materials characterizations. Thus, Li et al. (2018) and Sivakumar et al. (2017) identified the production of hydrogen peroxide at potentials of  $-0.5$  and  $-0.4$  V from nitrogen doped carbon@reduced graphene oxide and  $\text{V}_2\text{O}_5$  flakes, respectively. However, when this Fe-MOF was present, the peak was no longer observed, which can be due to the appearance of a wider region in the presence of the Fe-MOF that overlaps this peak and also may indicate the existing peroxide production was consumed by the Fenton reaction. The  $\text{Fe}^{2+}/\text{Fe}^{3+}$  redox couple could be found in the Fe-MOF@CB-PTFE-C curve (grey line). Thus, the presence of Fe in the MOF ( $\text{Fe}$ ) started the Fenton reaction and hydroxyl radicals were

produced through the following reaction (equation (5)) (Fdez-Sanromán et al., 2020).



According to literature, the catalytic production of  $\bullet\text{OH}$  by  $\text{H}_2\text{O}_2$  on several electro catalysts has been also proved. Thus, the CV curve after addition of  $\text{H}_2\text{O}_2$  using Fe/Mn@carbon cloth as cathode showed that co-doping can speed up the reaction rate of  $\text{H}_2\text{O}_2$  on the electrode, thus accelerating the  $\bullet\text{OH}$  formation (Li et al., 2022). Similarly, in our previous study (Cruz del Álamo et al., 2023) by the incorporation of perovskite by direct deposition over cathode surface induced the hydrogen peroxide decomposition into  $\bullet\text{OH}$ . Cui et al. (2020) determined by linear sweep voltammetry that the reduction of  $\text{H}_2\text{O}_2$  production of the composite cathode synthesized can be explained by the presence of  $\text{Fe}_3\text{O}_4$  nanoparticles.

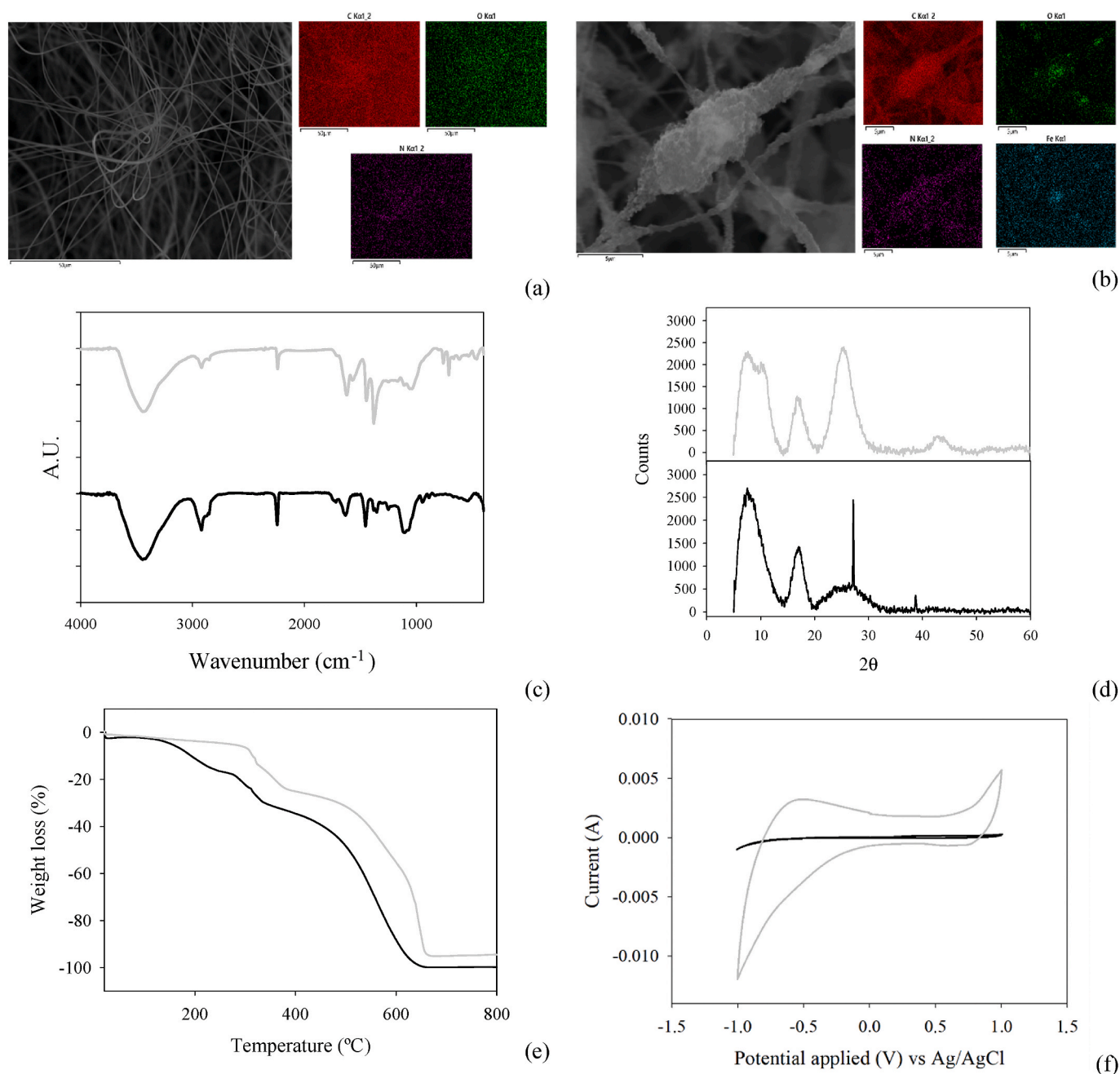


**Fig. 2.** SEM images and mappings of (a) PAN fibres and (b) Fe-MOF-CB@PAN fibres, (c) FTIR, (d) XRD, (e) TGA and (f) CV. Black and grey lines represent the results of PAN fibre and Fe-MOF-CB@PAN, respectively.

Thus, the obtained results demonstrated the potential of the proposed composite electrocatalyst for its application in an electro-Fenton treatment as first alternative.

### 3.2.2. Fe-MOF-CB@PAN-NF

According to section 2.2.2, initially, electrospinning was performed using different ratios of PAN, CB and Fe-MOF reagents to produce fibres. It was determined that using a ratio of PAN, CB and Fe-MOF of 7:5:2% (w/w) a Fe-MOF-CB@PAN fibre was successfully formed on NF surface (Fe-MOF-CB@PAN-NF). Prior its use as cathode, the fibre characterisation was carried out to assess its viability as electrocatalyst.

**3.2.2.1. Physicochemical characterisation.** The surface of the fibre electrode was analysed by electronic microscopy coupled with EDS and compared with a filamented PAN fibre (Fig. 2a and b). It can be easily observed the addition of CB and Fe-MOF changing the filaments morphology and, thus, the material's physical-chemical properties. The mapping of the Fe-MOF-CB@PAN displayed a higher carbon and iron content caused by the incorporation of CB and Fe-MOF into the PAN fibre.

These facts were also confirmed by FTIR analysis (Fig. 2c). In the Fe-MOF-CB@PAN samples, due to the synergistic effect of tensions between PAN, CB, and Fe-MOF, several peaks were more pronounced. Thus, the peaks detected between 1446 and 1381  $\text{cm}^{-1}$  were due to the symmetrical tension of the COO- and the bending of  $\text{CH}_2$  and  $\text{CH}_3$  groups. An aromatic CH bending and bond stresses between C-C, C-CN, and C-O fell within the range of 1151–1039  $\text{cm}^{-1}$ . This increase is largely due to active carbon as it favours more bonds of these types, especially C-O. As a matter of fact, Jiang et al. (2022) performed FTIR analysis of Fe-BTC immobilised on PAN. In this analysis, they fabricated a membrane containing a Fe-MOF of the same structure as the one used in this study. So, their FTIR analysis confirmed the correct assignment of the Fe-MOF, PAN, and CB peaks. Other characteristic peaks of PAN were also detected, such as the stresses of the O-H bonds between 3420 and 3443  $\text{cm}^{-1}$ , in addition to the tensions of the bond between nitrogen and carbon ( $\text{C}\equiv\text{N}$ ), which appeared at 2240  $\text{cm}^{-1}$ . It was also detected around the wavenumber of 2852–2965  $\text{cm}^{-1}$ , indicating tensions in the C-H bonds mainly due to the  $\text{CH}_2$ - $\text{CH}_3$  bonds (Hussain et al., 2021).

Regarding the XRD spectrum shown in Fig. 2d, it was possible to clearly distinguish the characteristic peaks of the PAN fibre (black line) and the Fe-MOF-CB@PAN fibre (grey line). It has been possible to identify as characteristic peaks of the PAN what appeared at  $2\theta$  on  $17^\circ$ ,  $27^\circ$  and  $40^\circ$ . These peaks were also found in the works of Jiang et al. (2022) and Samimi-Sohrforozani et al. (2021). When the Fe-MOF-CB@PAN fibre was analysed, only the peak of the PAN material was identified at  $2\theta = 17^\circ$ . In the case of the peaks  $2\theta = 26^\circ$  and  $2\theta = 43^\circ$  they were associated with the CB material, and the peak in  $2\theta = 11^\circ$  with the Fe-MOF. This was done with XRD characterisation of the composite electrode.

As in the case of the electrode composite, the same TGA analysis was performed (Fig. 2e). The two fibres presented a loss of mass between 50 and 200  $^\circ\text{C}$  due to intermolecular volatiles that are thought to be present within the PAN fibre, as Yang et al. (2022) showed with their pristine PAN nanofibers, or that provide the catalyst, as demonstrated previously in the Fe-MOF@CB-PTFE-C fibres. The next loss of mass, detected at a temperature above 280–360  $^\circ\text{C}$ , was due to the beginning of the decomposition of the PAN fibre. As Samimi-Sohrforozani et al. (2021) showed, this temperature can be slightly increased due to water content or when the fibre was doped with materials such as graphene oxide. As can be seen in Fig. 2e, the pure PAN fibre was completely degraded when a 600  $^\circ\text{C}$  temperature was reached. In contrast, Fe-MOF-CB@PAN-NF did not reach this level of decomposition due to the inorganic part of the fibre. This difference in behaviour was also found in the work of Yang et al. (2022), which compared pure PAN fibre with different ratios of bamboo shoot cellulose nanowhisker and carbon

nanotube. It showed that as the amount of these compounds increased, the final total decomposition of the material decreased. Furthermore, this behaviour was also analysed with the Fe-MOF@CB-PTFE-C material. It should be noted that because PAN was the main component of fibre, some of the mass losses due to CB and Fe-MOF, which was found in the grey curve of Fig. 1e, were not clearly reflected in the grey curve of Fig. 2e.

**3.2.2.2. Electrochemical characterisation.** In contrast to the previous characterizations, this CV compared the NF electrode with and without fibre revealing significant differences (Fig. 2f). The first was that the peaks found, around 0.4–0.6 V, in the NF, which corresponded to the Ni (II)/Ni (III) reduction pair, did not appear when covered by this fibre (Liu et al., 2017).

Another found difference was that the electrode covered by the fibre showed a change in behaviour at potentials applied below 0.2 V, as the current generated by this electrode was significant. One of the reasons for this change may be the incorporation of CB into the fibre. This increased the conductivity of the fibre produced from the NF. Similarly, it was reported that CB presence in modified graphite felt of Fe-Mn binary oxide increased the catalytic activity of oxygen reduction and the conductivity of cathode (Huang et al., 2021). Besides, it was detected a remarkably increase of the linear sweep voltammetry response, of the mixture of CB with Mn/Fe@porous carbon, could be attributed to the mutual promotion of CB and catalyst (Zhou et al., 2020). Due to these changes, NF could be used as supporting material to generate a cathode cover with fibre.

### 3.3. Antipyrine degradation using Fe-MOF functionalized cathodes

Both developed electrocatalysts that had been prepared and characterized were evaluated in the degradation of the antipyrine by electro-Fenton process.

#### 3.3.1. Fe-MOF@CB-PTFE-C

The feasibility of the developed electrocatalyst Fe-MOF@CB-PTFE-C was ascertained in the electro-Fenton process at different operational conditions of current density and initial pH (Fig. 3a).

The impact of current density is fundamental for the elimination of pollutant. Consistent with previous studies (Gao et al., 2020) the system had the highest pollutant removal efficiency operating at the lowest value. Thus, a pollutant removal of 35.6% and 32.43% were obtained for pH 7 and 3, respectively. These values sharply raised to 67.3 and 75.4%, respectively, when operating at 55.54  $\text{mA}/\text{cm}^2$ . Although electro-Fenton process produced better results at pH close to 3, the capability of the synthesized electrocatalyst to operate at natural pH without modification before the treatment, also avoids the need for subsequent effluent neutralization before discharging it into the environment.

The main explanation for these results may be that at high current intensities more hydrogen peroxide was produced. The differences in the results attained at different pH were very small proving the efficiency of the electrocatalyst in both conditions. It should be noted that Fe-MOF@CB-PTFE-C had a certain hydrophobicity with an average contact angle of  $103.13^\circ$ . Similar behaviour were found in the studies of Karatas et al. (2022) and Huang et al. (2021), in which CB and PTFE electrodes were synthesized. In both studies, it was reported that the hydrophobicity of these electrodes favoured peroxide production, which can be explained by the fact that the mass transference of oxygen in gas phase, supplied constantly through the bubbling, was higher and it reduced on the cathode to hydrogen peroxide. In addition, if more hydrogen peroxide was produced at pH close to 3, the electro-Fenton process was favoured so the removal of the pollutant would be higher. However, this was limited by the availability of the immobilised Fe-MOF to react. Only the catalyst allocated on the surface of the



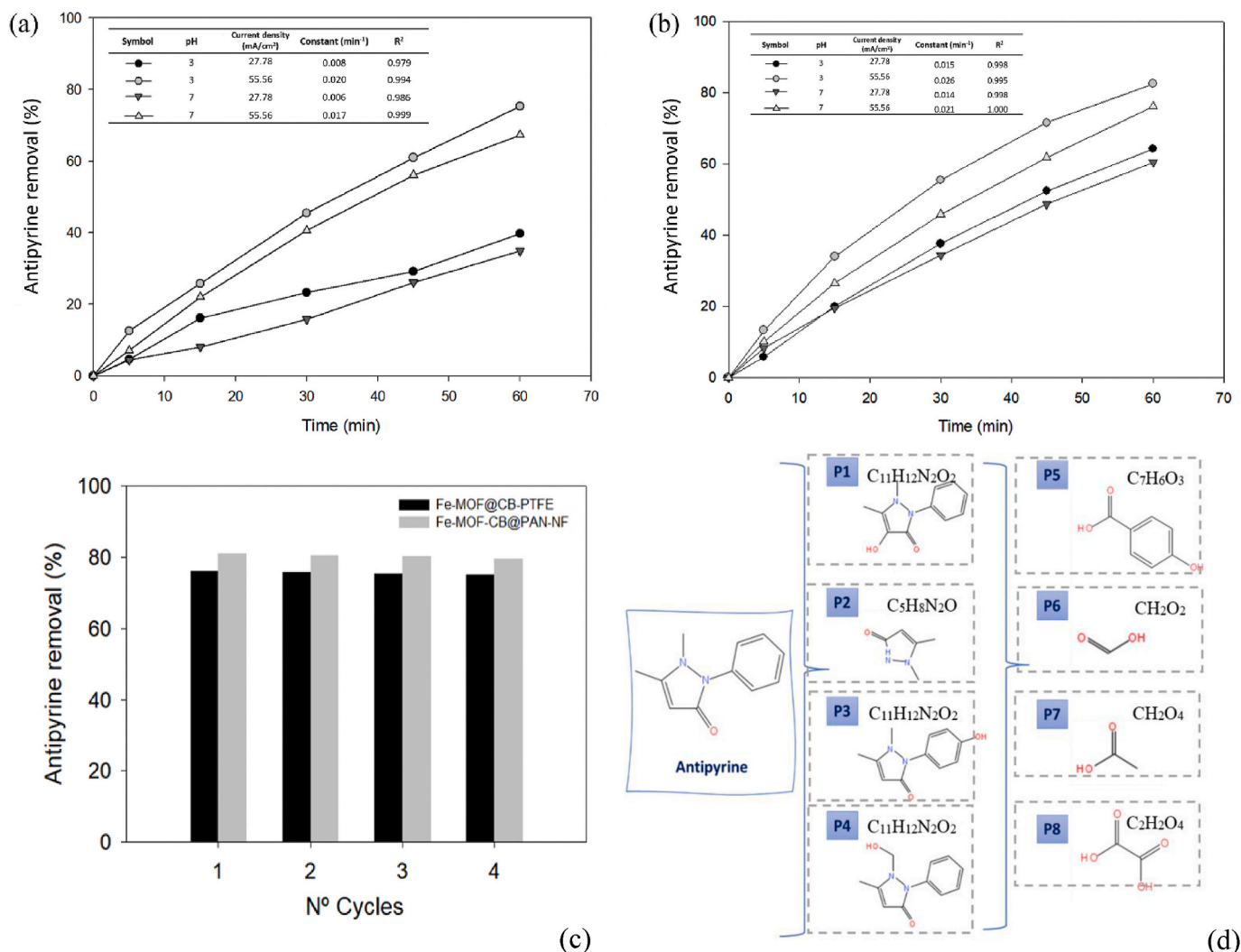


**Fig. 3.** Profile of antipyrine removal and first order kinetic parameters (inside figures) using (a) Fe-MOF@CB-PTFE-C and (b) Fe-MOF-CB@PAN-NF. (c) Reusing of the two Fe-MOF functionalized cathodes working at pH 3 and density 55.56 mA/cm<sup>2</sup> for 60 min. (d) As part of the electro-Fenton process, degradation products were identified, along with the corresponding antipyrine degradation route.

Fe-MOF@CB-PTFE-C, electrode will react as the surface hydrophobicity of the electrode did not allow the liquid to pass through and the Fenton reaction took place.

It is highlighted that the decomposition of antipyrine was due to the presence of Fe-MOF in Fe-MOF@CB-PTFE-C, as with CB-PTFE-C, the achieved elimination was less than half that obtained with the functionalized cathode. In the literature modified cathodes showed similar behaviour as in Dong et al. (2021). Thus, Fe (Fe-MOF, MIL-101) and Mn were selected for *in-situ* growth on the carbon fibre paper electrode CFP@MnO<sub>2</sub>-MIL-101. In this case, the difference between the control and the functionalized cathode (CFP@MnO<sub>2</sub>-MIL-101) was found 43.2% for the tetracycline degradation. The first order kinetic model fitted well to the experimental profiles obtained using CFP@MnO<sub>2</sub>-MIL-101 (0.0168 min<sup>-1</sup>) with similar values to ours results by Fe-MOF@CB-PTFE-C (0.02 min<sup>-1</sup>).

Thus, this cathode played a bifunctional role in the electro-Fenton process similar to the found by Xie et al. (2022) when rGO/MIL-88A/CF cathode was used. They accelerated the oxygen reduction reaction that occurred on the cathode to form the electro-generated H<sub>2</sub>O<sub>2</sub>, which can then be decomposed and activated simultaneously to form the  $\bullet$ OH radicals. The positive effect of the inclusion of MOF into the cathode was also determined by Wang et al. (2023) who synthesized a MOF-derived carbon material containing

CoFe alloy (Co/Fe@NPC) by calcining N-doped Co/Fe bimetallic MOF at a lower temperature. It was also confirmed that the degradation efficiency of ceftazidime gradually increased with the increase of applied current from 10 to 80 mA. Similar to our results, this fact could be explained due to higher application current density could effectively promote the production of H<sub>2</sub>O<sub>2</sub> and accelerate the recycling of  $\equiv$ Fe<sup>+2/+3</sup> (Liu et al., 2022).

### 3.3.2. Fe-MOF-CB@PAN-NF

To compare with previous Fe-MOF functionalized cathode, Fe-MOF-CB@PAN-NF electrocatalyst was also ascertained at the same working conditions (Fig. 3b).

Operating at the same pH, the removal efficiency was increased from 15.66% to 18.30% with the increase in current density. These results are explained by the fact that when the current density was increased, electron transfer becomes faster. This enhanced the oxygen reduction reaction and hydrogen peroxide production (Fdez-Sanromán et al., 2020, 2021). Additionally, the intensities tested enhanced anodic oxidation without secondary reactions that could reduce the current efficiency (Dinh et al., 2019).

As shown in Fig. 3b, the removal antipyrine efficiency at pH 3 and 55.56 mA/cm<sup>2</sup> was the highest, indicating a removal rate of 82.50%. The porosity of the electrode could explain this, as the hydrogen



peroxide in the aqueous medium more easily accessed the iron. Similar behaviour was found by Chen et al. (2019), who synthesized a sponge of zero-valent iron nanoparticles in a nanofiber network to remove sulfathiazole. The authors reported that the synthesized material was a highly porous sponge allowing having many catalytic active sites for the Fenton reaction took place. Furthermore, they mentioned that under acidic conditions the conversion of  $\text{Fe}^{+3}$  to  $\text{Fe}^{+2}$  on the surface was weakened and the release of iron species in the solution prevented. In this study, almost no iron leaching was detected (lower than 1%) and consequently with the heterogeneous catalysis being the main one.

When the prepared electrocatalyst (Fe-MOF@CB-PTFE-C and Fe-MOF@CB@PAN-NF) were compared, it can be observed that both resulted in good removals with the best conditions at acidic pH and higher current intensities attaining removal values around 80% in 1 h. Both electrocatalyst can operate at different pH and comparing the kinetic data shown in Fig. 3a and b, the process took place faster when Fe-MOF@CB@PAN-NF was used. Fe-MOF-CB@PAN-NF electrocatalyst showed slighter changes as a function of pH and current density. Similar behaviour was reported by Barhoum et al. (2021) who using nitrogen-doped carbon nanofiber electrodes incorporating Co/CoOx nanoparticles for the decolourization of Acid Orange 7 obtained very close results at a pH 3 and pH 6.

Several cycle reuses were performed (Fig. 3c) to analyse the stability of the Fe-MOF functionalized cathodes. Fig. 3c shows that both Fe-MOF functionalized cathodes were highly stable at low pH and high current. Throughout the four cycles, neither efficiency dropped below 5% nor energy consumption changed. This behaviour is similar than other electrocatalysts such as MIL-53(Fe)-MOF derived  $\text{Fe}_3\text{O}_4/\text{C}$  (MIL-53(Fe)@ $\text{Fe}_3\text{O}_4/\text{C}$ ) in which the CV analysis and reusability test of cathode catalyst showed only 8.03% drop of current density at the end of the 20th cycle and 5% drop of degradation efficiency after 6th cycle with low leaching of iron (Priyadarshini et al., 2023).

Because of their high stability along the time, the viability in their reuses and ability to remove persistent pollutants, Fe-MOF functionalized cathodes are promising alternatives. These cathodes manifest more cost-effective performance, lower energy consumption and higher oxygen utilization efficiency for  $\text{H}_2\text{O}_2$ , higher than gas diffusion electrodes (GDEs) (Wang et al., 2021).

### 3.4. Degradation products and toxicity estimation

The degradation intermediates of the electro-Fenton treatment for both electrocatalysts were followed. Eight antipyrine degradation products were detected in both cases (Fig. 3d). Some of these degradation products were understood to have cleavage mechanisms such as P1, which was obtained by hydroxylation of antipyrine, and P2, by phenylation. Both were found in Miao et al. (2015), in which antipyrine was removed using ozone. Two other products that were also produced by hydroxylation, P3 and P4, were found in the work of Gong et al. (2017). As in Gong et al. (2017) work, only mono-hydroxylation of antipyrine at different positions was detected and not di- or tri-hydroxylation products, which was corroborated because their retention times in HPLC-MS were close and they had the same chemical formula, as can be seen in Fig. 3d. With respect to P5, its detection could explain how antipyrine was broken to produce the products P2 and P5, since when the bond between the heterocycle and the aromatic ring was broken, these compounds were obtained, respectively. Finally, the products P6, P7 and P8 were small molecules resulting from the cleavage of the previous molecules and are common end products of advanced oxidation processes.

Once these degradation products were identified, three theoretical toxicological analyses of the products were performed using the TEST program: 96 h Fathead minnow LC50, 48 h *Daphnia magna* LC50 and oral rat LD50 (Table S4). The selected endpoints, including the Fathead minnow LC50, oral rat LD50, and *Daphnia magna* LC50, were chosen for their ability to provide crucial information regarding the potential harms and risks associated with substances to various organisms and

ecosystems. The Fathead minnow LC50 is instrumental in assessing the risk substances pose to fish populations, aiding in regulatory decisions aimed at environmental protection. On the other hand, the oral rat LD50 assists in determining safe exposure levels for humans, thereby guiding regulatory decisions concerning consumer product safety and occupational health. Lastly, the *Daphnia magna* LC50 is significant due to the species' importance in freshwater ecosystems, serving as an indicator of the potential impact of substances on non-target organisms.

According to the theoretical toxicological results for antipyrine, the initial concentration of the pollutant in the assays (50 mg/L) meant this value was higher than the determined by the *Daphnia magna* LC50 19.29 mg/L showing a short-term poisoning potential (acute toxicity). The same behaviour, with a value that could be over the toxicity threshold, was also observed for P1. When the other two theoretical toxicological analyses were considered, the selected initial concentration was below the determined thresholds, barely for Fathead minnow LC50 and significantly for oral rat LD50. The comparison was performed then between the antipyrine and the generated intermediates. As shown in Table S4, most of the detected intermediate products are less toxic than the parent compound for the three endpoints selected. Applying the *Daphnia magna* LC50, all degradation products are less hazardous than antipyrine (19.29 mg/L) and the determined concentrations were over the threshold value. However, for the Fathead minnow LC50 and oral rat LD50 models, it has been found that the P1 and P3 intermediates are slightly more toxic. Intermediate P1 only shows a higher toxicity (986.11 mg/L) in the oral rat LD50, while P3 has a higher toxicity in the two endpoints mentioned above (1011.32 mg/L oral rat LD50 and 25.18 mg/L Fathead minnow LC50). Anyway, all the intermediates concentration were below these determined values. However, to ensure this lower toxicity in aqueous media, further analyses are required.

## 4. Conclusions

In conclusion, the commercial Fe-MOF, Basolite® F-300, was shown to be an effective heterogeneous catalyst able to operate in suspension or as part of an electrocatalyst. In suspension, the relationship between pH, catalyst concentration, and current density was optimized to achieve the highest removal of antipyrine (94%) with low energy consumption (0.29 W·h per mg of antipyrine removed) under specific conditions: pH 3, Fe-MOF concentration of 157.78 mg/L, and current density of 6.67 mA/cm<sup>2</sup>. Moreover, two Fe-MOF immobilisation techniques were successfully developed for the preparation of electrocatalysts used as cathodes in electro-Fenton processes. The composites and fibres generated from these techniques showed promising results, with antipyrine elimination rates of 75.4% and 82.5%, respectively. The porous fibres offer a highly hydrophilic material that enhances the accessibility of Fe-MOF for the reactions, so further investigations are required to fully explore their potential. In addition, the intermediates have been determined and the toxicity of these products estimated to be less noxious than the parent compounds.

## Credit author statement

**Antía Fdez-Sanroman:** conceptualization, Investigation, Visualization. **Emilio Rosales:** Validation, Data curation, Supervision, Writing – review & editing. **Marta Pazos:** writing – review and editing, Project administration, Funding acquisition. **M. Angeles Sanromán:** Conceptualization, Methodology, Supervision, writing –review and editing, Project administration, Funding acquisition.

## Declaration of competing interest

The authors declare that they have no known competing financial interests or personal relationships that could have appeared to influence the work reported in this paper.

## Data availability

No data was used for the research described in the article.

## Acknowledgements

This research has been funded by R&D Project PID2020-113667 GB-I00 funded by MCIN/AEI/10.13039/501100011033 and PDC2021-121394-I00 funded by MCIN/AEI/10.13039/501100011033 and by the European Union Next Generation EU/PRTR. Xunta de Galicia and European Regional Development Fund (ED431C 2021–43). Moreover, Antía Fdez-Sanromán thanks MCIN/AEI/10.13039/501100011033 and FSE investing in your future for her predoctoral fellowship (PRE2021-098540). Funding for open access charge: Universidade de Vigo/CISUG.

## Appendix A. Supplementary data

Supplementary data related to this article can be found at <https://doi.org/10.1016/j.chemosphere.2023.139942>.

## References

- Barhoum, A., Favre, T., Sayegh, S., Tanos, F., Coy, E., Iatsunskyi, I., Razzouk, A., Cretin, M., Bechelany, M., 2021. 3D self-supported nitrogen-doped carbon nanofiber electrodes incorporated Co/CoO(x) nanoparticles: application to dyes degradation by electro-fenton-based process. *Nanomaterials* 11, 2686. <https://doi.org/10.3390/nano11102686>.
- Brillas, E., 2022. Progress of homogeneous and heterogeneous electro-Fenton treatments of antibiotics in synthetic and real wastewaters. A critical review on the period 2017–2021. *Sci. Total Environ.* 819, 153102 <https://doi.org/10.1016/j.scitotenv.2022.153102>.
- Casado, J., 2019. Towards industrial implementation of Electro-Fenton and derived technologies for wastewater treatment: a review. *J. Environ. Chem. Eng.* 7, 102823 <https://doi.org/10.1016/j.jece.2018.102823>.
- Chen, L., Fan, S., Xiong, P., Song, J., Dai, Q., 2021. Catalytic ozonation of antipyrine with a magnetic core/shell cocatalyst: kinetics and mechanism. *Desalination Water Treat.* 212, 444–451. <https://doi.org/10.5004/dwt.2021.26723>.
- Chen, Y.-P., Yang, L.-M., Paul Chen, J., Zheng, Y.-M., 2019. Electrospun spongy zero-valent iron as excellent electro-Fenton catalyst for enhanced sulfathiazole removal by a combination of adsorption and electro-catalytic oxidation. *J. Hazard Mater.* 371, 576–585. <https://doi.org/10.1016/j.jhazmat.2019.03.043>.
- Conde-González, J.E., Lorenzo-Luis, P., Salvadó, V., Havel, J., Peña-Méndez, E.M., 2021. A new cotton functionalized with iron (III) trimer-like metal framework as an effective strategy for the adsorption of triarylmethane dye: an insight into the dye adsorption processes. *Heliyon* 7. <https://doi.org/10.1016/j.heliyon.2021.e08524>.
- Cruz del Álamo, A., Puga, A., Pariente, M.I., Rosales, E., Molina, R., Pazos, M., Martínez, F., Sanromán, M.A., 2023. Activity and stability of bifunctional perovskite/carbon-based electrodes for the removal of antipyrine by electro-Fenton process. *Chemosphere* 334, 138858. <https://doi.org/10.1016/j.chemosphere.2023.138858>.
- Cuervo Lumbaque, E., Cardoso, R.M., de Araújo Gomes, A., Malato, S., Sánchez Pérez, J. A., Sirtori, C., 2021. Removal of pharmaceuticals in hospital wastewater by solar photo-Fenton with Fe<sup>3+</sup>-EDDS using a pilot raceway pond reactor: transformation products and in silico toxicity assessment. *Microchem. J.* 164, 106014 <https://doi.org/10.1016/j.microc.2021.106014>.
- Cui, L., Huang, H., Ding, P., Zhu, S., Jing, W., Gu, X., 2020. Cogeneration of H<sub>2</sub>O<sub>2</sub> and OH via a novel Fe<sub>3</sub>O<sub>4</sub>/MWCNTs composite cathode in a dual-compartment electro-Fenton membrane reactor. *Sep. Purif. Technol.* 237, 116380 <https://doi.org/10.1016/j.seppur.2019.116380>.
- Deblonde, T., Cossu-Leguillie, C., Hartemann, P., 2011. Emerging pollutants in wastewater: a review of the literature. *Int. J. Hyg Environ. Health* 214, 442–448. <https://doi.org/10.1016/j.ijheh.2011.08.002>.
- Dinh, C.-T., Jain, A., de Arquer, F.P.G., De Luna, P., Li, J., Wang, N., Zheng, X., Cai, J., Gregory, B.Z., Voznyy, O., Zhang, B., Liu, M., Sinton, D., Crumlin, E.J., Sargent, E.H., 2019. Multi-site electrocatalysts for hydrogen evolution in neutral media by destabilization of water molecules. *Nat. Energy* 4, 107–114. <https://doi.org/10.1038/s41560-018-0296-8>.
- Dong, P., Chen, X., Guo, M., Wu, Z., Wang, H., Lin, F., Zhang, J., Wang, S., Zhao, C., Sun, H., 2021. Heterogeneous electro-Fenton catalysis with self-supporting CFP@MnO<sub>2</sub>-Fe<sub>3</sub>O<sub>4</sub>/C cathode for shale gas fracturing flowback wastewater. *J. Hazard Mater.* 412, 125208 <https://doi.org/10.1016/j.jhazmat.2021.125208>.
- Du, X., Fu, W., Su, P., Zhang, Q., Zhou, M., 2023. FeMo@porous carbon derived from MIL-53(Fe)/MoO<sub>3</sub> as excellent heterogeneous electro-Fenton catalyst: Co-catalysis of Mo. *J. Environ. Sci.* 127, 652–666. <https://doi.org/10.1016/j.jes.2022.06.031>.
- Du, X., Wang, S., Ye, F., Qingrui, Z., 2022. Derivatives of metal-organic frameworks for heterogeneous Fenton-like processes: from preparation to performance and mechanisms in wastewater purification – a mini review. *Environ. Res.* 206, 112414 <https://doi.org/10.1016/j.envres.2021.112414>.
- Du, X., Zhou, M., 2021. Strategies to enhance catalytic performance of metal–organic frameworks in sulfate radical-based advanced oxidation processes for organic pollutants removal. *Chem. Eng. J.* 403, 126346 <https://doi.org/10.1016/j.cej.2020.126346>.
- Fdez-Sanromán, A., Acevedo-García, V., Pazos, M., Sanromán, M.Á., Rosales, E., 2020. Iron-doped cathodes for electro-Fenton implementation: application for pyrimethamine degradation. *Electrochim. Acta* 338, 135768. <https://doi.org/10.1016/j.electacta.2020.135768>.
- Fdez-Sanromán, A., Martínez-Treinta, R., Pazos, M., Rosales, E., Sanromán, M.Á., 2021. Heterogeneous electro-fenton-like designs for the disposal of 2-phenylphenol from water. *Appl. Sci.* 11, 12103 <https://doi.org/10.3390/app112412103>.
- Fdez-Sanromán, A., Pazos, M., Sanromán, A., 2022. Peroxymonosulphate activation by basolite F-300 for Escherichia coli disinfection and antipyrine degradation. *Int. J. Environ. Res. Publ. Health* 19, 6852. <https://doi.org/10.3390/ijerph19116852>.
- Gao, Y., Zhu, W., Wang, C., Zhao, X., Shu, M., Zhang, J., Bai, H., 2020. Enhancement of oxygen reduction on a newly fabricated cathode and its application in the electro-Fenton process. *Electrochim. Acta* 330, 135206. <https://doi.org/10.1016/j.electacta.2019.135206>.
- Gomes, I.B., Madureira, D., Simões, L.C., Simões, M., 2019. The effects of pharmaceutical and personal care products on the behavior of Burkholderia cepacia isolated from drinking water. *Int. Biodeterior. Biodegrad.* 141, 87–93. <https://doi.org/10.1016/j.ibiod.2018.03.018>.
- Gong, H., Chu, W., Chen, M., Wang, Q., 2017. A systematic study on photocatalysis of antipyrine: catalyst characterization, parameter optimization, reaction mechanism a toxicity evolution to plankton. *Water Res.* 112, 167–175. <https://doi.org/10.1016/j.watres.2017.01.041>.
- Gou, Y., Ma, J., Yang, S., Song, Y., 2022. Insights into the effects of Fenton oxidation on PAH removal and indigenous bacteria in aged subsurface soil. *Environ. Pollut.* 298, 118872 <https://doi.org/10.1016/j.envpol.2022.118872>.
- Hondred, P.R., Yoon, S., Bowler, N., Kessler, M.R., 2013. Degradation kinetics of polytetrafluoroethylene and poly(ethylene-alt-tetrafluoroethylene). *High Perform. Polym.* 25, 535–542. <https://doi.org/10.1177/0954008312473491>.
- Huang, A., Zhi, D., Zhou, Y., 2021. A novel modified Fe–Mn binary oxide graphite felt (FMBO-GF) cathode in a neutral electro-Fenton system for ciprofloxacin degradation. *Environ. Pollut.* 286, 117310 <https://doi.org/10.1016/j.envpol.2021.117310>.
- Hussain, M., Salam, A., Arain, M.F., Ullah, A., Dao, A.T., Vu-Manh, H., Phan, D.N., Ansari, A.S., Khan, M.Q., Javed, Z., Kim, I.S., 2021. Polyacrylonitrile nanofibers containing virobloc as promising material for protective clothing. *Appl. Sci.* 11, 11469 <https://doi.org/10.3390/app112311469>.
- Jiang, G., Jia, Y., Wang, J., Sun, Y., Zhou, Y., Ruan, Y., Xia, Y., Xu, T., Xie, S., Zhang, S., Ye, X., 2022. Facile preparation of novel Fe-BTC@PAN nanofibrous aerogel membranes for highly efficient continuous flow degradation of organic dyes. *Sep. Purif. Technol.* 300, 121753 <https://doi.org/10.1016/j.seppur.2022.121753>.
- Karatas, O., Gengec, N.A., Gengec, E., Khataee, A., Koby, M., 2022. High-performance carbon black electrode for oxygen reduction reaction and oxidation of atrazine by electro-Fenton process. *Chemosphere* 287, 132370. <https://doi.org/10.1016/j.chemosphere.2021.132370>.
- Lama, G., Meijide, J., Sanromán, A., Pazos, M., 2022. Heterogeneous advanced oxidation processes: current approaches for wastewater treatment. *Catalysts* 12, 344. <https://doi.org/10.3390/catal12030344>.
- Lee, S.M., Lee, S.H., Roh, J.S., 2021. Analysis of activation process of carbon black based on structural parameters obtained by XRD analysis. *Crystals* 11, 1–11. <https://doi.org/10.3390/cryst11020153>.
- Li, Y., Wang, C., Pan, S., Zhao, X., Liu, N., 2022. Mn doping improves in-situ H<sub>2</sub>O<sub>2</sub> generation and activation in electro-Fenton process by Fe/Mn@CC cathode using high-temperature shock technique. *Chemosphere* 307, 136074. <https://doi.org/10.1016/j.chemosphere.2022.136074>.
- Li, Z., Jiang, Y., Wang, Z., Wang, W., Yuan, Y., Wu, X., Liu, X., Li, M., Dilpazir, S., Zhang, G., Wang, D., Liu, C., Jiang, J., 2018. Nitrogen-rich core-shell structured particles consisting of carbonized zeolitic imidazolate frameworks and reduced graphene oxide for amperometric determination of hydrogen peroxide. *Microchim. Acta* 185, 501. <https://doi.org/10.1007/s00604-018-3032-y>.
- Liu, W., Wu, X., Li, X., 2017. Gold nanorods on three-dimensional nickel foam: a non-enzymatic glucose sensor with enhanced electro-catalytic performance. *RSC Adv.* 7, 36744–36749. <https://doi.org/10.1039/c7ra06909j>.
- Liu, Z., Wan, J., Yan, Z., Wang, Y., Ma, Y., 2022. Efficient removal of ciprofloxacin by heterogeneous electro-Fenton using natural air–cathode. *Chem. Eng. J.* 433, 133767 <https://doi.org/10.1016/j.cej.2021.133767>.
- Miao, H.-F., Cao, M., Xu, D.-Y., Ren, H.-Y., Zhao, M.-X., Huang, Z.-X., Ruan, W.-Q., 2015. Degradation of phenazone in aqueous solution with ozone: influencing factors and degradation pathways. *Chemosphere* 119, 326–333. <https://doi.org/10.1016/j.chemosphere.2014.06.082>.
- Nguyen, M.B., Nga, D.T.N., Thu, V.T., Piro, B., Truong, T.N.P., Yen, P.T.H., Le, G.H., Hung, L.Q., Vu, T.A., Ha, V.T.T., 2021. Novel nanoscale Yb-MOF used as highly efficient electrode for simultaneous detection of heavy metal ions. *J. Mater. Sci.* 56, 8172–8185. <https://doi.org/10.1007/s10853-021-05815-3>.
- Ouiriemmi, I., Escudero-Curiel, S., Pazos, M., Angeles Sanromán, M., 2022. On-site regeneration by ultrasound activated persulfate of iron-rich Antipyrine-loaded biochar. *J. Environ. Chem. Eng.* 10, 108400 <https://doi.org/10.1016/j.jece.2022.108400>.
- Peñas-Garzon, M., Gómez-Avilés, A., Belver, C., Rodríguez, J.J., Bedia, J., 2020. Degradation pathways of emerging contaminants using TiO<sub>2</sub>-activated carbon heterostructures in aqueous solution under simulated solar light. *Chem. Eng. J.* 392, 124867 <https://doi.org/10.1016/j.cej.2020.124867>.

- Pisharody, L., Gopinath, A., Malhotra, M., Nidheesh, P.V., Kumar, M.S., 2022. Occurrence of organic micropollutants in municipal landfill leachate and its effective treatment by advanced oxidation processes. *Chemosphere* 287, 132216. <https://doi.org/10.1016/j.chemosphere.2021.132216>.
- Poza-Nogueiras, V., Gomis-Berenguer, A., Pazos, M., Sanroman, A., Ania, C.O., 2022. Exploring the use of carbon materials as cathodes in electrochemical advanced oxidation processes for the degradation of antibiotics. *J. Environ. Chem. Eng.* 10, 107506 <https://doi.org/10.1016/j.jece.2022.107506>.
- Poza-Nogueiras, V., Rosales, E., Pazos, M., Sanromán, M.A., 2018. Current advances and trends in electro-Fenton process using heterogeneous catalysts - a review. *Chemosphere* 201, 399–416. <https://doi.org/10.1016/j.chemosphere.2018.03.002>.
- Priyadarshini, M., Ahmad, A., Ghangrekar, M.M., 2023. Efficient upcycling of iron scrap and waste polyethylene terephthalate plastic into Fe<sub>3</sub>O<sub>4</sub>@C incorporated MIL-53(Fe) as a novel electro-Fenton catalyst for the degradation of salicylic acid. *Environ. Pollut.* 322, 121242 <https://doi.org/10.1016/j.envpol.2023.121242>.
- Reddersen, K., Heberer, T., Dünnebier, U., 2002. Identification and significance of phenazone drugs and their metabolites in ground- and drinking water. *Chemosphere* 49, 539–544. [https://doi.org/10.1016/S0045-6535\(02\)00387-9](https://doi.org/10.1016/S0045-6535(02)00387-9).
- Rivera-Torrente, M., Filez, M., Hardian, R., Reynolds, E., Seoane, B., Coulet, M.V., Oropeza Palacio, F.E., Hofmann, J.P., Fischer, R.A., Goodwin, A.L., Llewellyn, P.L., Weckhuysen, B.M., 2018. Metal-organic frameworks as catalyst supports: influence of lattice disorder on metal nanoparticle formation. *Chem. Eur. J.* 24, 7498–7506. <https://doi.org/10.1002/chem.201800694>.
- Sai, V., Ramireddy, R., Kurakula, R., Velayudhaperumal, P., James, A., Hullebusch, E.D. Van, 2023. Systematic computational toxicity analysis of the ozonolytic degraded compounds of azo dyes: quantitative structure-activity relationship (QSAR) and adverse outcome pathway (AOP) based approach. *Environ. Res.* 231, 116142 <https://doi.org/10.1016/j.envres.2023.116142>.
- Samimi-Sohrforozani, E., Azimi, S., Abolhasani, A., Malekian, S., Arbab, S., Zendeheh, M., Abolhasani, M.M., Yaghoobi Nia, N., 2021. Development of porous polyacrylonitrile composite fibers: new precursor fibers with high thermal stability. *Electron. Mater.* 2, 454–465. <https://doi.org/10.3390/electronicmat2040031>.
- Shamsudin, M.S., Mohammad, M., Zobir, S.A.M., Asli, N.A., Bakar, S.A., Abdullah, S., Yahya, S.Y.S., Mahmood, M.R., 2013. Synthesis and nucleation-growth mechanism of almost catalyst-free carbon nanotubes grown from Fe-filled sphere-like graphene-shell surface. *J. Nanostructure Chem.* 3, 13. <https://doi.org/10.1186/2193-8865-3-13>.
- Sippel, T.R., Son, S.F., Groven, L.J., 2013. Altering reactivity of aluminum with selective inclusion of polytetrafluoroethylene through mechanical activation. *Propellants, Explos. Pyrotech.* 38, 286–295. <https://doi.org/10.1002/prep.201200102>.
- Sirés, I., Brillas, E., 2021. Upgrading and expanding the electro-Fenton and related processes. *Curr. Opin. Electrochem.* 27, 100686 <https://doi.org/10.1016/j.coelec.2020.100686>.
- Sivakumar, M., Sakthivel, M., Chen, S.M., Veeramani, V., Chen, W.L., Bharath, G., Madhu, R., Miyamoto, N., 2017. A facile low-temperature synthesis of V<sub>2</sub>O<sub>5</sub> flakes for electrochemical detection of hydrogen peroxide sensor. *Ionics* 23, 2193–2200. <https://doi.org/10.1007/s11581-017-2046-5>.
- Sun, S., Diao, P., Feng, C., Ungureanu, E.M., Tang, Y., Hu, B., Hu, Q., 2018. Nickel-foam-supported β-Ni(OH)<sub>2</sub> as a green anodic catalyst for energy efficient electrooxidative degradation of azo-dye wastewater. *RSC Adv.* 8, 19776–19785. <https://doi.org/10.1039/c8ra03039a>.
- Ursueguía, D., Díaz, E., Ordóñez, S., 2020. Densification-induced structure changes in basolite mofs: effect on low-pressure CH<sub>4</sub> adsorption. *Nanomaterials* 10, 1089. <https://doi.org/10.3390/nano10061089>.
- Wang, H., Tang, C., Wang, L., Sun, Z., Hu, X., 2023. MOF-derived Co/Fe@NPC-500 with large amounts of low-valent metals as an electro-Fenton cathode for efficient degradation of ceftazidime. *Appl. Catal. B Environ.* 333, 122755 <https://doi.org/10.1016/j.apcatb.2023.122755>.
- Wang, J., Li, C., Rauf, M., Luo, H., Sun, X., Jiang, Y., 2021. Gas diffusion electrodes for H<sub>2</sub>O<sub>2</sub> production and their applications for electrochemical degradation of organic pollutants in water: a review. *Sci. Total Environ.* 759, 143459 <https://doi.org/10.1016/j.scitotenv.2020.143459>.
- Xie, F., Gao, Y., Zhang, Jingbin, Bai, H., Zhang, Jianfeng, Li, Z., Zhu, W., 2022. A novel bifunctional cathode for the generation and activation of H<sub>2</sub>O<sub>2</sub> in electro-Fenton: characteristics and mechanism. *Electrochim. Acta* 430, 141099. <https://doi.org/10.1016/j.electacta.2022.141099>.
- Yang, Y., Gao, M., Wu, Y., Liu, Z., Xie, J., Deng, Z., Cai, G., Cao, X., Ke, W., 2022. Fabrication and characterization of electrospun polyacrylonitrile (PAN)/bamboo shoot cellulose nanowhisker (BSCNs)/carbon nanotube (CNT) composite membrane with enhanced dye adsorption properties. *Cellulose* 29, 3817–3827. <https://doi.org/10.1007/s10570-022-04531-8>.
- Zhou, X., Xu, D., Chen, Y., Hu, Y., 2020. Enhanced degradation of triclosan in heterogeneous E-Fenton process with MOF-derived hierarchical Mn/Fe@PC modified cathode. *Chem. Eng. J.* 384, 123324 <https://doi.org/10.1016/j.cej.2019.123324>.